

Review

Probing Active Sites on Metal-Free, Nitrogen-Doped Carbons for Oxygen Electoreduction: A Review

Ni Zhou ^{1,†}, Nan Wang ^{1,†}, Zexing Wu ² and Ligui Li ^{1,3,*} 

¹ Guangzhou Key Laboratory for Surface Chemistry of Energy Materials, New Energy Research Institute, School of Environment and Energy, South China University of Technology, Guangzhou Higher Education Mega Center, Guangzhou 510006, China; eszn@mail.scut.edu.cn (N.Z.); eswangnan@mail.scut.edu.cn (N.W.)

² State Key Laboratory Base of Eco-chemical Engineering, College of Chemistry and Molecular Engineering, Qingdao University of Science & Technology, 53 Zhengzhou Road, Qingdao 266042, China; splswzx@qust.edu.cn

³ Guangdong Provincial Key Laboratory of Atmospheric Environment and Pollution Control, School of Environment and Energy, South China University of Technology, Guangzhou 510006, China

* Correspondence: esguili@scut.edu.cn; Tel.: +86-20-3938-0520

† These authors contribute equally to this work.

Received: 30 September 2018; Accepted: 30 October 2018; Published: 1 November 2018



Abstract: The Metal-free nitrogen-doped carbons represent an emerging low-cost nonprecious electrocatalyst for oxygen reduction reaction (ORR) that is a sluggish process at the cathode of polymer electrolyte membrane fuel cells (PEMFCs) and a verity of metal-air batteries. During the past few years, the ORR catalytic activity of nitrogen-doped carbons has been significantly increased, making them highly competitive alternatives to conventional precious metals based electrocatalysts for ORR. However, controversies remain in the unambiguous identification of the ORR active sites on nitrogen-doped carbons. This review summarizes the recent progress in probing the potential active sites on metal-free nitrogen-doped carbons for ORR, aiming to gain in-depth understanding of the ORR catalytic mechanism on nitrogen-doped carbons for further enhancing ORR activity.

Keywords: oxygen reduction reaction; active site; nitrogen-doped carbon; electrocatalytic activity; fuel cells

1. Introduction

The emerging energy crisis and global climatic issues have impelled scientists and engineers to explore renewable energy technologies [1], of which PEMFC has become one research hotspot due to various advantages, such as using renewable and green hydrogen as a fuel, high power conversion efficiency, high energy density [2] and so on. However, the cathodic ORR usually shows a sluggish charge-transfer kinetics which requires efficient electrocatalysts to boost. Normally, precious Pt based nanomaterials are the universal choice of ORR electrocatalysts [3]. However, the apparent disadvantages of Pt based precious metals, such as scarcity and high cost, heavily impede the widespread commercialization of PEMFC technology. Alternatively, many cost-effective electrocatalysts have been developed during the past few decades, including the low-cost transition metals and nitrogen codoped carbons (M-N/C, M = Fe or Co) [4], metal oxides [5,6], transition metal carbides [7], nitrides [8,9], chalcogenides [10], perovskites [11,12], and also metal-free heteroatom doped carbon based electrocatalysts [13]. Comparing to metal containing electrocatalysts, the metal-free carbon-based materials demonstrate many advantages, such as widely available precursors, environmentally friendly, strong resistance to the poisoning of CO and high immunity to the negative impacts from fuel crossover. Among them, N-doped carbons have attracted intensive research attentions due to their remarkable ORR catalytic activity.

Normally, there are four nitrogen doping configurations on carbon skeletons, i.e., pyridinic N, pyrrolic N, graphitic (or quarterly) N and oxidized N (Figure 1), with a binding energy of 398.2, 399.4, 400.8 and 402.7 eV, respectively [14]. Bonding with two carbon atoms at the boundary or defect of graphene, pyridinic N possesses a lone pair of electrons and donates one p electron to the π system. In regard to pyrrolic N, the N atom substitutes a carbon atom of the five-membered ring and donates two p electrons to the π system. Graphitic N refers to an N atom which bonds to three carbon atoms in carbon of hexagonal ring planes, and it is less impressionable to the protonation reaction because of an unavailable lone pair of electrons around N atom in the carbon plane.

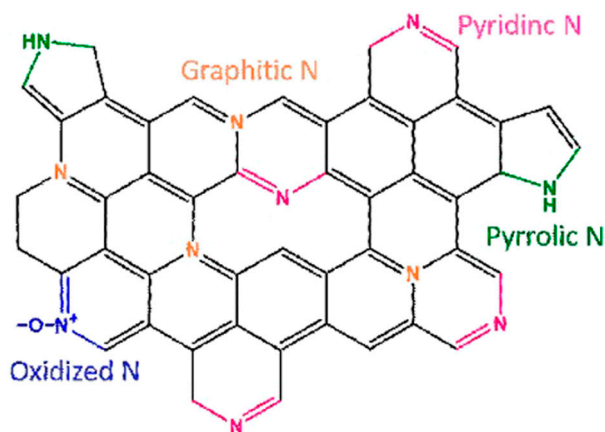


Figure 1. The four nitrogen doping configurations usually observed on carbon catalysts.

Recent researches reveal that doping nitrogen atoms to carbon skeletons can markedly influence the charge distribution on adjacent carbon atoms, and the oxygen chemisorption mode is changed consequently [15–17]. Although the nitrogen doping strategy has been proven to be effective in improving the ORR activity in various carbon-based materials, including carbon nanosphere [18], nanotube [19], graphene [20,21], etc., the intrinsic active sites for catalyzing ORR on the nitrogen-doped carbons haven't been conclusively identified and thus probing the ORR on N-doped carbons remains a hot research topic. In other words, despite that oxidized N is generally believed to be inert, whether the other three nitrogen doping configurations (i.e., pyrrolic N, pyridinic N or graphitic N) dominate ORR activity of N-doped carbons or not remains a matter of active debates. Several factors are considered to account for this situation: (i) Coexistence of different N doping structures in N-doped carbon electrocatalysts. So far, selectively generating only one specific nitrogen doping configuration on the entire carbon matrix during the synthesis procedure is still an enormous challenge which makes it an intractable issue to unambiguously determine the direct correlation between the definite nitrogen doping configuration (e.g., pyrrolic N, graphitic N or pyridinic N) and ORR activity. (ii) The ORR activity of N-doped carbons is also influenced by multiple structural parameters, including morphology, graphitization level, defect, relative work function on interface, and composition etc.; and the internal heterogeneity of the electrocatalysts often further complicates this issue. (iii) N-doped carbon samples prepared from the same group can also have fluctuations in structure and activity.

In the present review, we summarize the recent important reports on probing ORR active sites on metal-free, N-doped carbon nanomaterials to gain a deeper insight into the mechanism of ORR which will be conducive to promote the synthesis of more efficient carbon-based ORR electrocatalysts.

2. Dopant-Free Carbon Nanomaterials

Because structural defects and edges are usually widely present in N-doped carbons, it is necessary to summarize the progress in identifying the active sites for ORR on dopant-free carbons. Regarding carbon-based materials, intrinsic carbon can also play a significant role in the electrocatalytic process. For instance, Gong et al. systematically studied different electrochemical processes on

sidewalls and tips of ultra-long (about 5 mm) perpendicularly aligned carbon nanotube (CNT) arrays by selectively depositing an insulating polymer coating layer on nanotube tip(s) or sidewalls, respectively. They found that depending on the electrochemical species involved, both the tip and sidewall of nanotube could have prominent impact on the electrochemistry of CNT electrode [22].

As for ORR in alkaline electrolyte, Wang and co-workers delicately studied the corresponding ORR activity of edge and basal planes by precisely depositing a tiny air-saturated droplet at prescribed location on highly oriented pyrolytic graphite (HOPG) [23]. Experimentally, electrochemical characterizations were also performed by using a three-electrode configuration, where the reaction system was comprised of a working electrode of HOPG, a counter electrode of a Pt wire fixed in a capillary tube, and a reference electrode of an Ag/AgCl wire (Figure 2a). After comparing the ORR activities of air-saturated droplets deposited on the locations with multiple steps (edges) (Figure 2b) and basal plane (without steps) (Figure 2c), they found that the graphite located at basal plane displayed an inferior limiting current density and onset potential than the one at the edge (Figure 2d). It is believed that the intrinsic ORR catalytic activity of edges on HOPG is attributed to the presence of higher charge density and delocalized charge on edge/defect carbon atoms. This is the first unambiguous report which shows that carbon atoms at the edge are more active and it enlightens researchers to develop edge/defect rich carbon-based catalysts.

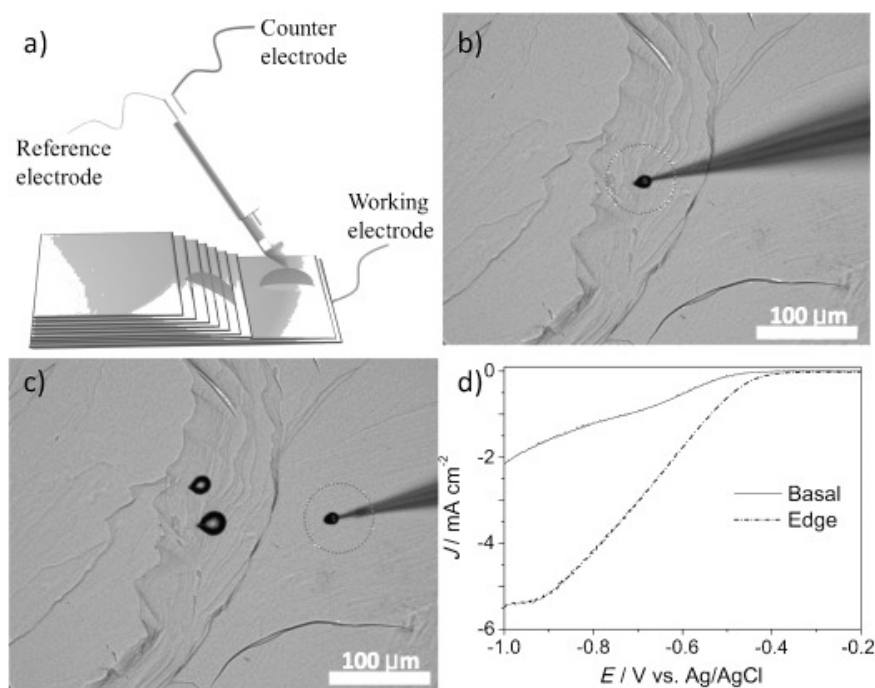


Figure 2. (a) Schematic illustration of the micro appliance for the oxygen reduction reaction (ORR) activity analysis. Optical image for showing the highly oriented pyrolytic graphite (HOPG) substrate serving as a working electrode by placing an air-saturated electrolyte droplet on (b) the edge and (c) the basal plane of HOPG. (d) LSV curves for ORR proceeded in an air-saturated electrolyte deposited either on the edge (see panel b) or on the basal plane (see panel c) of HOPG. (Reprinted with permission from Ref. [23], 2014 WILEY-VCH).

Recently, Yao and co-workers successfully synthesized dopant-free defect-rich graphene (DG) after completely removing nitrogen atoms via heating N-containing carbon precursor under 1150 °C (Figure 3) [24], which showed trifunctional electrocatalytic activities, including ORR, oxygen evolution reaction (OER) and hydrogen evolution reaction (HER). High-resolution transmission electron microscopy (HR-TEM) images clearly revealed the reconstruction of carbon and formation of various carbon defects, including pentagons, heptagons, and octagons. These defects are believed to account

for the ORR activity [25,26] not only because they can modulate the electronic environment around the vacancies, but also promote the wetting properties owing to the changes in surface area and surface hydrophobicity after perturbing the surface properties of graphene.

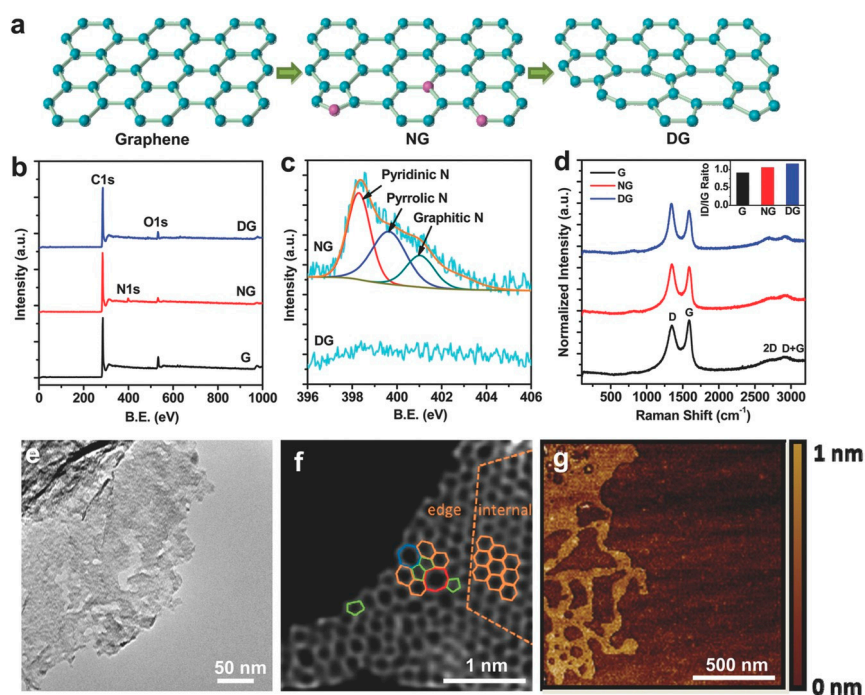


Figure 3. (a) Schematic illustration of the synthesis process of defect-rich graphene (DG). (b) X-ray photoelectron spectroscopy (XPS) spectra of the pristine graphene, NG, and DG. (c) The corresponding high-resolution N1s XPS spectra of NG as well as DG. (d) Raman spectra of pristine graphene, NG, and DG. (e) TEM image of DG sample. (f) HAADF image of DG sample determined at an accelerated voltage of 80 kV. Hexagons (orange), pentagons (green), heptagons (blue), and octagons (red) (g) The representative atomic force microscopy (AFM) image of DG sample. (Figures are reprinted with permission from Ref. [24], 2016 WILEY-VCH).

Apart from the edge sites, intrinsic carbon defects are also explored in order to ascertain the intrinsic active sites for ORR on carbons. Hu et al. synthesized carbon nanocages with pentagon, hole, and edge defects by in-situ MgO template method [27]. In their experiments, dangling bonds of all the edged carbon atoms were eliminated by hydrogenation (Figure 4). From the thermodynamic viewpoint, the zigzag edge and pentagon defects were considered as the potential ORR active sites according to density functional theory (DFT) calculation, while the hole defects, armchair edges and pristine sp^2 carbon atoms are inert to ORR. According to their results, the zigzag edge defects have a portion of the active unpaired π electrons that can effectively facilitate electron transfer to O_2 and hence exhibit lower free energy for in the formation of OOH^* species as compared with the pristine sp^2 carbon. This result signifies that the edge defects and non-hexagonal topological defects may contribute to the increase of ORR activity for holy carbons. Along this line, Dai and co-workers used Ar plasma to treat dopant-free graphene, which helped create structure defects but reserve its high electronic conductivity [28]. The thus-obtained defect- and edge-rich graphene indeed demonstrated remarkably enhanced ORR activity as compared with the pristine graphene. Moreover, DFT calculations also indicate that the high charge density on edge- and defect-carbon atoms most likely accounts for the apparent ORR activity for dopant-free carbons.

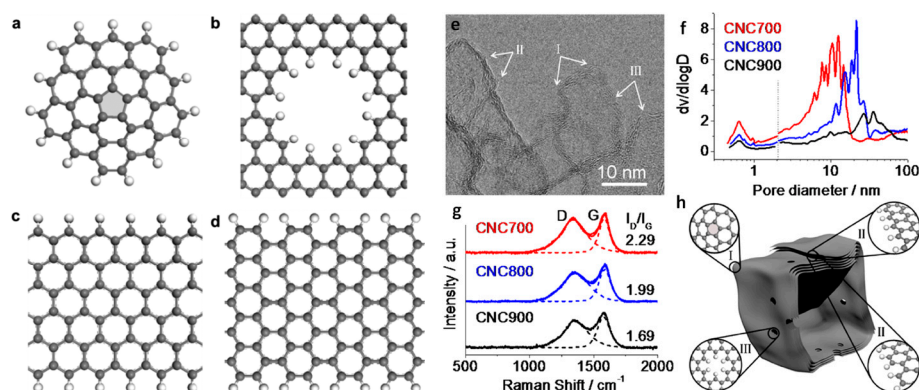


Figure 4. Defect models of (a) Pentagon (highlight), (b) Hole, (c) Zigzag edge and (d) Armchair-like edge. C atom (gray), H atom (white). (e) Representative HR-TEM image of CNC700. (f) Pore size distributions for different samples. (g) The corresponding Raman spectra of CNC. (h) Schematic illustration of a carbon nanocage structure with three typical defective locations I (the corner), II (the broken fringe) and III (the hole). Reprinted with permission from Ref. [27], 2015 American Chemical Society.

3. N-Doped Carbon Nanomaterials

A large number of N-doped carbon-based nanomaterials have been published during the past few years, including graphene, graphite, carbon nanospheres, carbon nanotubes and so on. These various N-doped carbon nanomaterials can even rival commercial Pt/C catalysts in terms of ORR electrocatalytic activity but with a much lower cost and more widely available earth-abundant precursor materials [29]. As mentioned above, although many promising N-doped carbon electrocatalysts for ORR have been prepared, researchers have not reached a consensus on discrimination of the active sites. Herein, we summarize the recent important progress in probing the ORR catalytic active sites on representative N-doped carbon nanomaterials, aiming to help understand the ORR mechanism, and also better design and synthesize more efficient carbon electrocatalysts.

A pioneer work in N-doped carbon electrocatalysts for ORR was conducted by Gong and co-workers in 2009, where perpendicularly aligned nitrogen-containing carbon nanotubes (referred as VA-NCNTs) (Figure 5a,c) were prepared by simple pyrolysis of the iron(II) phthalocyanine [15]. These NCNTs are observed to show a zigzag-like path along the nanotube axial direction and doping nitrogen into the graphitic texture generated a bamboo-like feature. The metal-free VANCNTs were obtained by electrochemical purification to remove the residual Fe and the resulting catalyst exhibited a four-electron ORR procedure in alkaline electrolyte. Interestingly, the electrocatalytic activity and working stability of metal-free VANCNTs were even higher while the overpotential and fuel crossover effect were lower than that of commercially available Pt/C catalyst. On the basis of the quantum mechanics calculation results, Gong et al. pointed out that a considerably high positive charge density of carbon atoms was able to counterbalance the strong electronic affinity of the neighboring nitrogen atoms (Figure 5d). Correspondingly, the chemisorption mode of oxygen can be changed by nitrogen-induced charge delocalization from the usual end-on adsorption (Pauling model, see the top sketch in Figure 5e) on undoped CNTs to a side-on adsorption (Yeager model, see the bottom sketch in Figure 5e) on NCNTs surface, which can significantly weaken the O–O bond to facilitate ORR. Therefore, introduction of nitrogen, an element that has a stronger electron affinity than C not only helps modify the surface electronic configuration for carbon-based electrocatalysts but also furthermore incubate additional active sites and defects for catalyzing ORR.

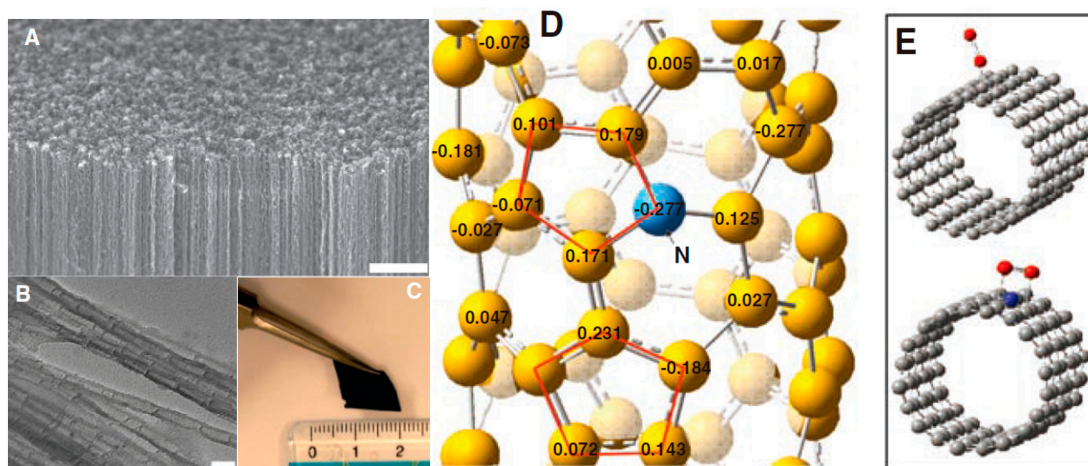


Figure 5. (A) The SEM image for showing the side-view of as-prepared VA-NCNTs deposited on a quartz surface. (B) The TEM image for showing the morphology of the VA-NCNTs which have been electrochemically purified. (C) The digital photograph of the VA-NCNT array after having been transferred onto a conductive nanocomposite film. (D) The charge density distribution on the NCNTs according to DFT calculations. (E) Sketch for showing the potential chemical adsorption modes of a single oxygen molecule on undoped CNTs (top) and NCNTs (bottom). Reprinted with permission from Ref. [15], 2009, American Association for the Advancement of Science.

In addition to directly doping carbon skeletons with nitrogen, an alternative method was subsequently developed by Wang et al., where they found that the positively charged polyelectrolyte such as Poly-diallyl dimethylammonium chloride (PDDA) showed a vigorous electron-withdrawing capability and could create net positive and delocalized charges on the conjugated graphene surface when adsorbing onto the surface of graphene [30], leading to intermolecular charge transfer states. Consequently, the graphene catalyst adsorbing positively charged PDDA exhibits a much higher ORR electrocatalytic activity than wholly graphene (Figure 6a). Besides, Wang et al. also employed the positively charged PDDA to tune the ORR catalytic activity of pristine CNTs [31]. Electrons of electrons-rich carbon atoms on CNTs can be withdrawn by the functional groups (i.e., quaternary ammonium) on PDDA backbone, resembling the introduction of a p-type dopant, and therefore the positively charged carbon atoms can not only enhance the oxygen adsorption but also facilitate ORR through potent attraction of electrons from the anode (Figure 6b). These observations signify a vital function of intermolecular charge transfer in carbon and it seems that carbon atoms could also serve as the active sites for ORR.

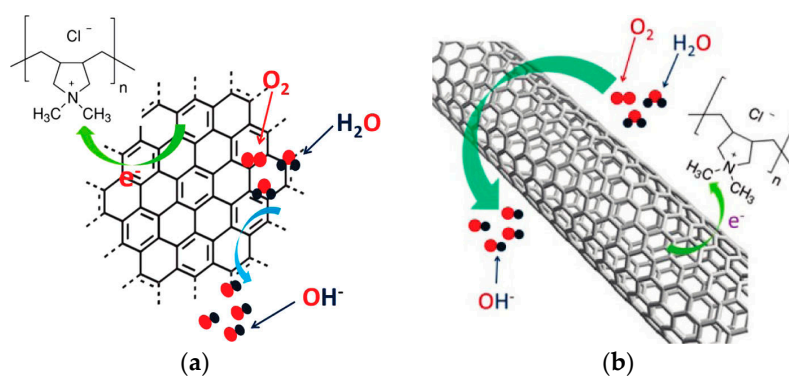


Figure 6. (a) Schematic illustration of the PDDA-induced electron-withdrawing interaction on graphene. (Reprinted with permission from Ref. [30], 2011 American Chemical Society) (b) Schematic illustration of charge transfer and ORR process on PDDA-CNT composite. Reprinted with permission from Ref. [31], 2011 American Chemical Society.

These results clearly demonstrated that the introduction of nitrogen doping or topological defects to carbon can reallocate the electron density within the carbon structure, thus leading to electron fluctuations on the carbon surface and improving oxygen adsorption. As mentioned above, the three main nitrogen doping configurations on carbon skeletons, including graphitic N, pyrrolic N and pyridinic N are regarded as potential active sites for catalyzing ORR, while the oxidized N is generally inactive. For pyridinic N and pyrrolic N, they are connected with two sp^2 hybridized C atoms, while graphitic N (i.e., quaternary N) is directly bonded with three tetrahedral sp^3 hybridized C atoms [32]. The planar sp^2 hybridization of C–N bond shows a torsion angle of 0° while the tetrahedral sp^3 hybridization is observed to show a torsion angle of 60° [33], hence pyrrolic N and pyridinic N usually show a planar platelet structure while quaternary N generally displays an uneven (three dimensional) structure. With a quasi-closed flat nanoreactor comprised of layered montmorillonite (MMT), Wei and co-workers synthesized pyrrolic N and pyridinic N-doped graphene (NG) which could selectively generate planar N via adjusting the interspace width of the MMT flat nanoreactor [34]. In their synthesis experiment (Figure 7), aniline (AN) monomers were first intercalated into the layers of MMT, and then in situ oxidation polymerization was performed, followed by high-temperature pyrolysis. High content (90.27%) of planar N (pyridinic N and pyrrolic N) is selectively generated and well-preserved by the MMT flat nanoreactor, leading to enhanced electrical conductivity as proven by the results of electrochemical impedance spectroscopy measurements as well as considerable ORR catalytic activity. The authors concluded that both pyridinic N and pyrrolic N are more active for ORR electrocatalysis than graphitic N which might benefit from the high electrical conductivity attributed to the reservation of planar structures after nitrogen doping. Although this conclusion still requires further support from the straight correlation between the ORR performance and a specific N, one can find that nitrogen doping configuration influences the local structure of carbon materials and hence finally on the corresponding ORR activity.

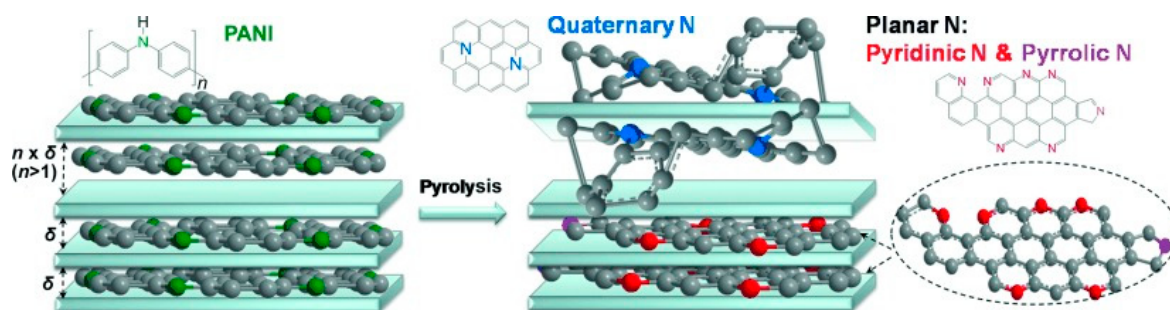


Figure 7. Schematically showing the controlled synthesis of N-doped carbons comprising different nitrogen doping configurations with MMT serving as nanoreactor. Reprinted with permission from Ref. [34], 2013 WILEY-VCH.

It is worth knowing that apart from the structure effects derived from nitrogen doping, topological defect is also proven to influence on ORR electrocatalytic activity. Recently, Zhang et al. synthesized edge-rich N-doped graphene mesh via direct carbonization of sticky rice with the presence of nitrogen source melamine and $Mg(OH)_2$ nanosheet hard templates [35]. DFT calculations were performed to probe the possible ORR active sites derived from many structure factors, including nitrogen-doping, topological defects, and edge effects, for instance pyrrolic N, pyridinic N and quaternary N on the edge (Q), quaternary N in the bulk phase (QN), five-carbon ring (C5), seven-carbon ring (C7), as well as five-carbon ring wired to seven-carbon ring (C5+7) as depicted in Figure 8a. They found that for all nitrogen doping-caused sites, the sites neighboring to the edge exhibited a much lower overpotential in ORR catalysis, signifying the strong influence of edge effects on ORR. Topological defects (e.g., pentagon and heptagon carbon rings) can significantly diminish the overpotential of ORR in the DFT computation as compared with pristine graphene, and these nitrogen-free configurations that are contiguous to pentagonal and heptagonal carbon rings display the minimum overpotential

as depicted in Figure 8b, locating the summit of volcano plots for both ORR and oxygen evolution reaction (OER). Based on their DFT results, the interacted O and OOH species preferably bind at the junction of the rings comprised of neighboring seven-carbon and five-carbon, whereas the O–O bond in OOH species are tend to be broken by the C5–C7 dipole in the C5+7 configuration and engender a facile reduction of oxygen (Figure 8c). It is believed that the discrepancy of electron densities induced by contiguous carbon rings is capable of developing spatial curvatures and further generating a permanent dipole moment. Therefore, a moderate adsorption might account for the higher ORR activity of the C5+7 configurations rather than that between nitrogen and carbon atoms because of the presence of stronger dipole moment. Also, the free energy diagrams of ORR sub-steps on active sites reveal the determining step is transformation of O* to OH* for pyrrolic N while desorption of OH[−] from C5+7 serves as the determining step (Figure 8d,e), further suggesting that the C5+7 defect promotes adsorption of oxygen intermediates. These results remind us of the importance of topological defects and provide a path to further understanding the active sites for ORR.

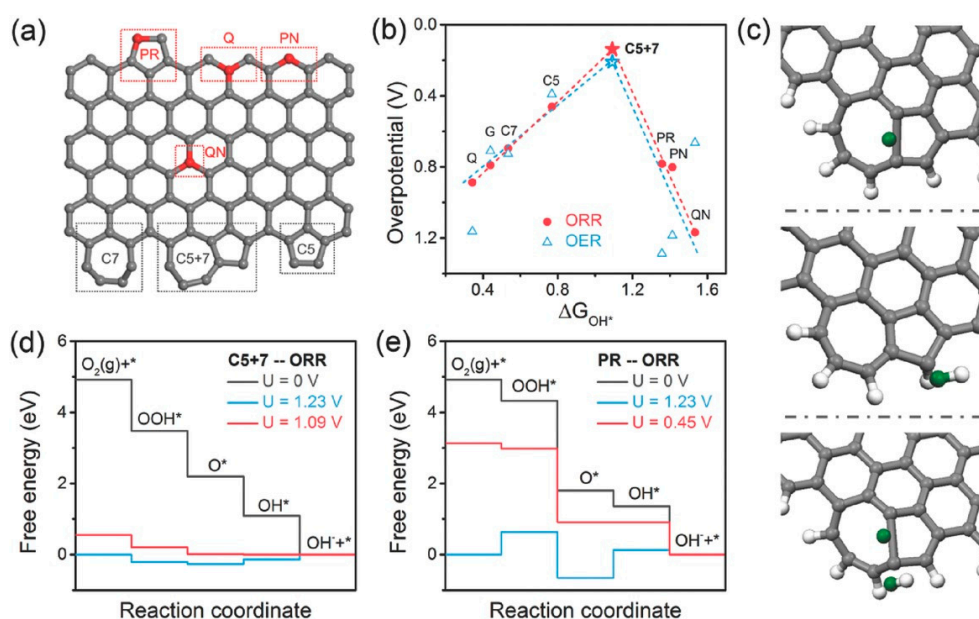


Figure 8. (a) Schematic illustration of various kinds of N-doping types or topological defects on graphene skeleton. (PR: pyrrolic nitrogen; PN: Pyridinic nitrogen.) (b) Volcano plots of overpotential versus adsorption energy of OH* for ORR and OER. (c) Schematic illustration of optimized adsorption mode of C5+7 interacting with O, OH, and OOH species (from top to bottom). Diagrams for showing the calculated free energy for ORR proceeded at pH = 0 on (d) graphene with C5+7 defect and (e) pyrrolic N. The color of elements: carbon (gray), hydrogen (white), oxygen (blue), and nitrogen (red). Reprinted with permission from Ref. [35], 2016 WILEY-VCH.

Recently, several research groups advocated that the potential active site for ORR is pyridinic N among the N-doped carbon catalysts [36–39]. Li et al. proposed that the analysis and identification of the chemical composition of nitrogen-doped graphene before and after ORR might be an optional method to determine the active sites [40]. The change of graphitic, pyrrolic and pyridinic N contents for three representative samples were tracked by X-ray photoelectron spectroscopy (XPS) spectra for nitrogen-doped multilayer graphene through determination of the chemisorbed oxygen reduction intermediates (Figure 9a–f). As a sort of the intermediates of ORR, –OH attached to aromatic carbon was increased to a higher content after the ORR process, and it led to an upshift in the binding energy of the nitrogen from 398.8 to 400.2 eV [41]. Moreover, they observed that the XPS intensity of the pyridinic peak gradually decreased as the ORR proceeded while the intensity of the “pyrrolic” nitrogen increased (Figure 9g–h). Therefore, they inferred that the diminishment ORR activity could be correlated with the transformation of the pristine pyridinic N to the pyrrolic N, and the increase of

XPS intensity for pyrrolic N peak might be due to the incremental content of the OH-attached pyridinic N instead of pyrrolic N. They also found that N-doped carbon with the highest content of OH(ads) attached to the carbon atoms neighboring to pyridinic N after ORR showed the best ORR catalytic performance among the series; hence, they concluded that pyridinic N had a significant impact on ORR activity.

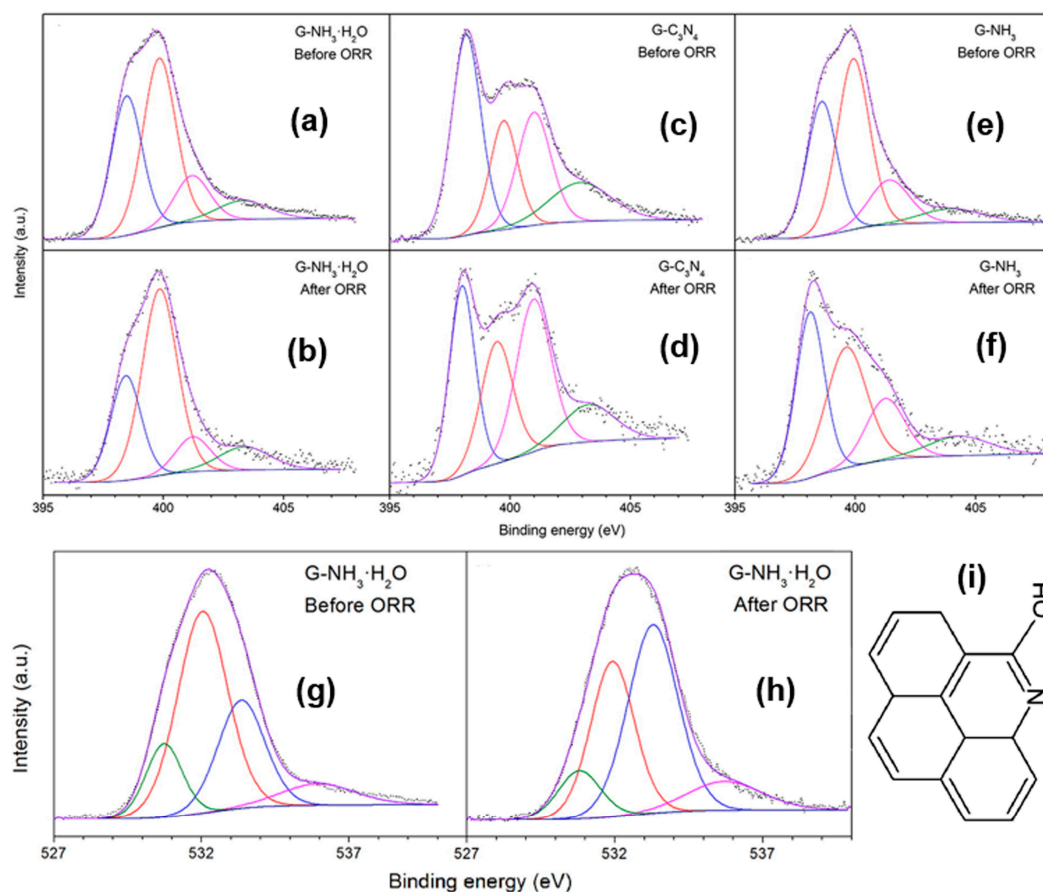


Figure 9. (a–f) The corresponding high-resolution XPS N1s spectra of the three multilayer graphene samples obtained before and after ORR. The least-squares fitted peaks are pyrrolic N at 399.8 eV (red), graphitic N at 401.2 eV (purple), pyridinic N at 398.5 eV (blue), and nitrogen oxide at 403 eV (green). XPS O1s spectra of G-NH₃·H₂O obtained (g) before and (h) after ORR. The fitted peaks are C=O at 530.8 eV (green), C(aliphatic)-OH/C(aliphatic)-O-C(aliphatic) at 532.0 eV (red), C(aromatic)-OH at 533.3 eV (blue), and chemisorbed water molecules at 535.7 eV (purple). (i) Diagram of the chemical structure of –OH attached to the pyridinic N. Reprinted with permission from Ref. [40] 2014 American Chemical Society.

As mentioned above, N-doped carbon nanomaterials usually concurrently contain multiple nitrogen-doping configurations; hence, it is difficult to discern the direct correlation between a specific nitrogen doping configuration and ORR activity. To alleviate the impacts of these structural factors, recently, Guo et al. used model catalysts HOPG (i.e., highly oriented pyrolytic graphite) with controlled nitrogen doping conjugations and well-defined π conjugation to probe the ORR active sites in a 0.1-M H₂SO₄ aqueous solution [42]. The edge-HOPG samples prepared by bombarding the HOPG with an Ar⁺ ion beam through a thin metallic mask were utilized to synthesize the Pyridinic N-dominated HOPG model catalysts through thermal annealing in NH₃ atmosphere, while the graphitic N-dominated HOPG model catalysts were prepared by thermally annealing the HOPG that had been subjected to mild bombardment with a nitrogen ion beam. They found that although the nitrogen concentration of the pyri-HOPG sample was lower than that of the grap-HOPG sample

(Figure 10a), its ORR activity was much higher than that of grap-HOPG as depicted in Figure 10b, and the apparent ORR current density for the series control samples showed a linear dependence on the content of pyridinic N. Because the pyri-HOPG sample is nearly absolutely comprised with pyridinic N (95% for pyridinic N and 5% for graphitic N), Guo et al. concluded that pyridinic N could reduce the ORR overpotential more efficiently than Graphitic N, and hence pyridinic N was most likely the ORR active site. Further investigation of the intermediates of ORR by ex situ post-ORR XPS measurements revealed that the content of nitrogen decreased after ORR (Figure 10c) and the OH species-attached carbon atoms next to pyridinic N led to conversion of the pyridinic N to pyridonic N (Figure 10d). Additionally, the results of CO₂ temperature programmed desorption (CO₂-TPD) measurements showed that the acidic CO₂ molecule preferentially adsorbed on pyri-HOPG (Figure 10e), indicative of the formation of Lewis base sites on pyri-HOPG. Previous DFT calculations showed that the carbon atoms contiguous to pyridinic N could act as active Lewis bases for its tendency to donate electron pairs [43]. Oxygen molecules were reported to adsorb on Lewis base sites [44]. Because the first step of the whole ORR process is adsorption of O₂, Guo et al. proposed that the active site for ORR could be a Lewis base site derived from pyridinic N.

However, graphitic N was recently suggested to be responsible for the ORR active sites rather than pyridinic N and pyrrolic N. For example, Yang et al. used melamine and L-cysteine as precursors to synthesize 3D metal-free N-doped graphene nanoribbon networks (N-GRW) that consisted of a high nitrogen content and showed active ORR and OER bi-functional catalytic activities and conducted active site probing experiments in alkaline electrolytes [45]. Mott-Schottky analysis experiments were performed and revealed that N-GRW had high charge carrier density. According to ultraviolet photoelectron spectroscopy (UPS) spectra, a smaller work function in valence band emission region was obtained for N-GRW, which demonstrates that there is a lower energetic barrier, i.e., a higher driving energy, for the electron transfer from catalyst to the adsorbed oxygen. Herein, the rate-determining step for ORR catalysis which is regarded to promote the formation of OOH species. From the X-ray absorption near-edge structure (XANES) spectra of carbon (Figure 11b) and nitrogen (Figure 11c) elements before and after oxygen reduction, one can find that after ORR or OER, the peak intensity associated with p^{*}C–O–C, C–N in Figure 11b increased at 287.7 eV, indicating that the intermediate species (O^{*}) were adsorbed on the carbon atoms, and a new peak arose at 289.6 eV after ORR and OER, corresponding to the adsorption of OOH^{*} intermediates. Meanwhile, as depicted in Figure 11c, the nitrogen K-edge XANES spectrum of the N-GRW after ORR, displayed a new peak which is close to graphitic N (~401 eV) but with a lower binding energy. Such a new peak was attributed to O^{*} and OOH^{*} intermediates adsorbed on carbon atoms surrounding graphitic N and leads to distortion of heterocycles. In sharp contrast, the peak of pyridinic N at around 398.0 eV remained unchanged after ORR, as compared with the pristine N-GRW (Figure 11c). Based on these results, Yang et al. concluded that the active N-doping configuration for the ORR is likely to be quaternary N with n-type doping nature, rather than pyridinic N with p-type doping characteristic on the N-GRW electrode. They also pointed out that the augmentation of nucleophile strength for the carbon atoms surrounding quaternary N was attributed to the reason that quaternary N could provide partial electrons to the highly conjugated carbon skeleton (i.e., n-type doping), which could facilitate the adsorption of oxygen molecule onto the carbon skeleton surface and, hence, promote ORR process. Interestingly, they found that the pyridinic N species served as the electrocatalytic active sites for OER.

More recently, our group conducted prolonged potential cycling on three representative N-doped carbons synthesized with the methods reported by three different groups in O₂-saturated 0.1 M KOH aqueous solution in order to probe the ORR active sites and attempt to shield the influence of different morphology, defect, graphitization level etc. on discriminating the interrelationship between definite nitrogen doping configurations and ORR performance [14]. The limiting current was found to be attenuated closely correlated with the diminishment of graphitic N content, as supported by the results of XPS spectra and Mott-Schottky analysis. Interestingly, among all the three model catalysts, the prolonged electrochemical potential cycling nearly had no influence on the specific activity per

graphitic N within a wide-range of potentials which was consistent with the theoretical prediction (Figure 12). In sharp contrast, no such interrelationship was identified for both pyrrolic N and pyridinic N.

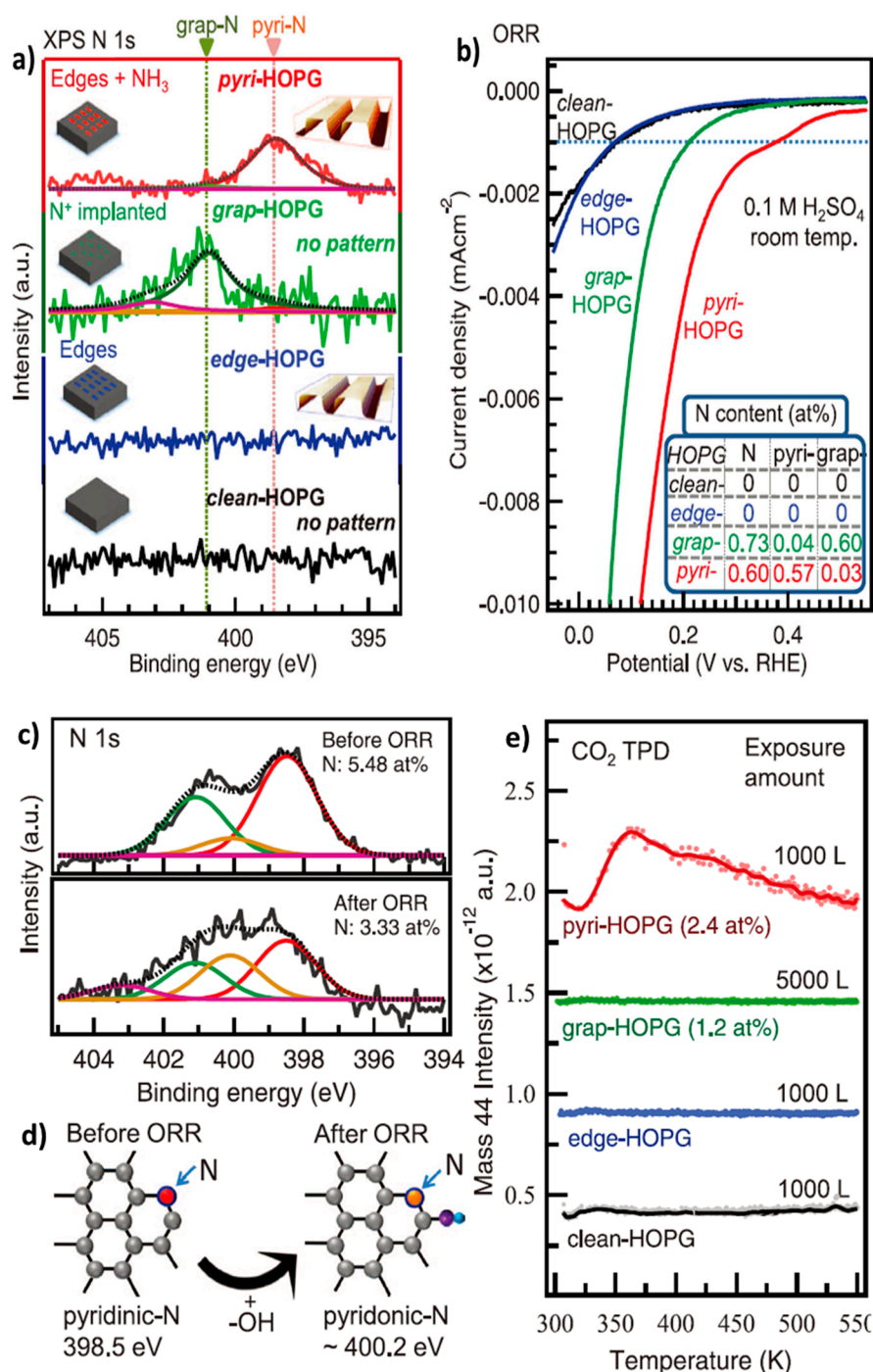


Figure 10. (a) The high-resolution N 1s XPS spectra determined for model catalysts. (b) The ORR catalytic results for model catalysts depicted in panel (a). Inset to the panel is nitrogen contents corresponding to the model catalysts. (c) N 1s XPS spectra of the N-HOPG model catalyst before and after ORR, respectively. (d) Schematic illustration of the formation of pyridonic N by the attachment of OH to the carbon atom adjacent to pyridinic N. (e) CO₂-TPD results of the HOPG model catalysts. Reprinted with permission from Ref. [42], 2016, American Association for the Advancement of Science.

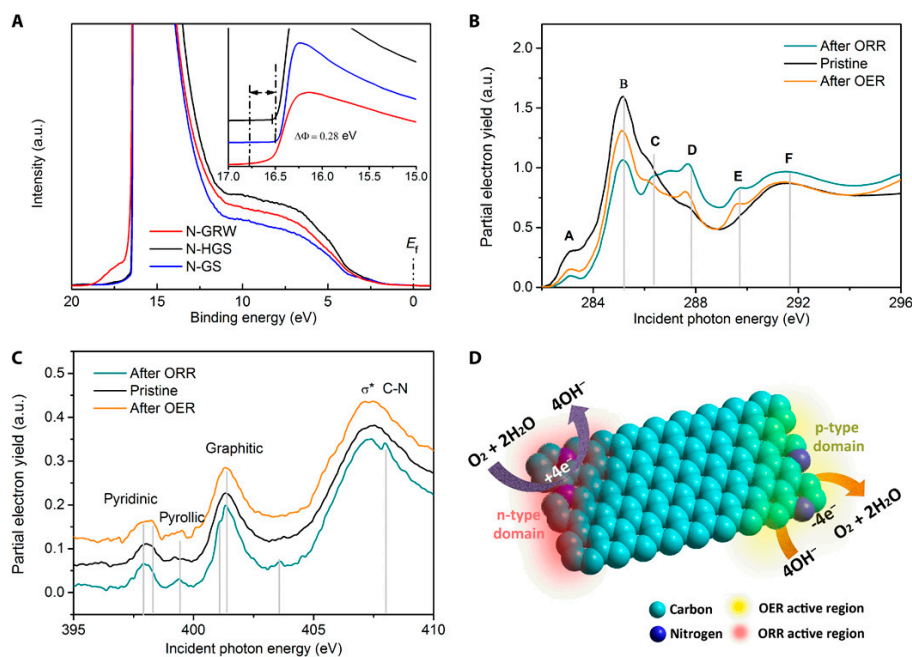


Figure 11. (A) UPS spectra collected using an He I (21.2 eV) radiation. Secondary electron tail threshold was enlarged and exhibited in the inset. (B,C) Carbon and nitrogen K-edge XANES spectra of N-GRW catalyst. In carbon K-edge XANES spectra, A: defects, B: $\pi^*C=C$, C: π^*C-OH , D: π^*C-O-C , C-N, E: $\pi^*C=O$, COOH, F: σ^*C-C . (D) Schematic diagram of the N-GRW catalyst. n- and p-type domains carried different active sites for ORR and OER. Reprinted with permission from Ref. [45].

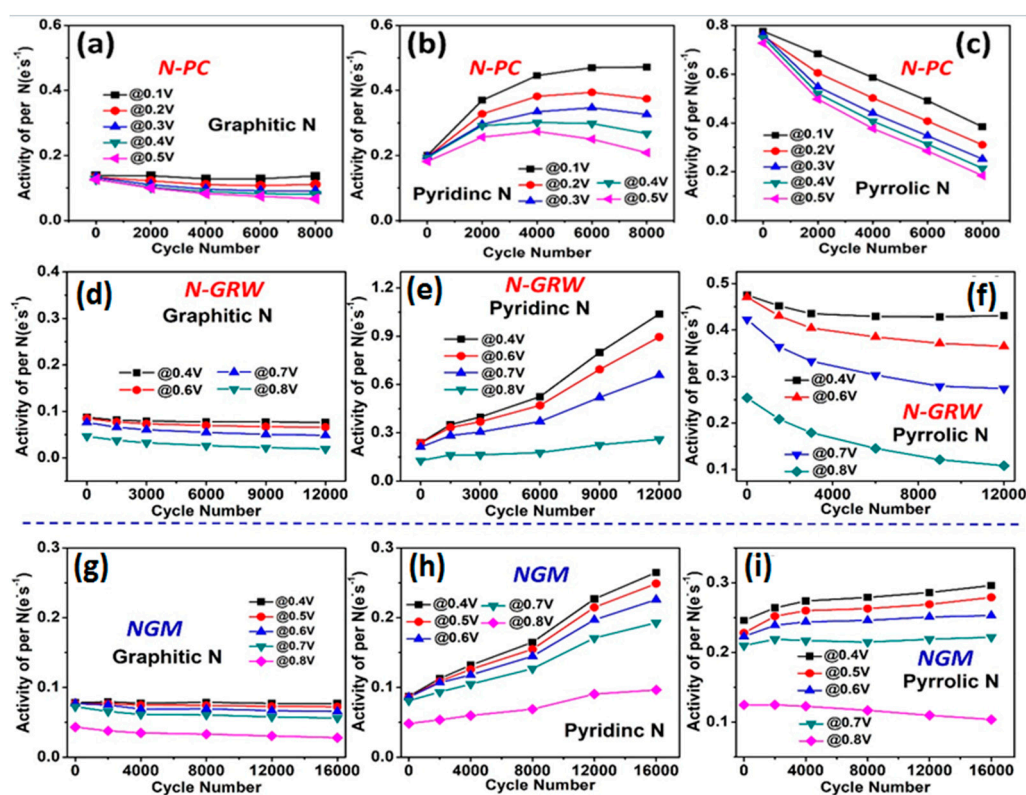


Figure 12. Plots for showing the evolution of specific activity against cycling number for (a,d,g) graphitic N, (b,e,h) pyridinic N and (c,f,i) pyrrolic N in (a–c) N-PC (d–f) N-GRW and (g–i) NGM.

Furthermore, Gibbs free energy change of the first-electron reduction, regarded as a rate-determining step for the $4e^-$ ORR process (Figure 13a), proceeded on carbons surrounding

pyridinic or pyrrolic N was much higher than the one on carbon atoms contiguous to graphitic N (Figure 13b), according to the calculations of density functional theory (DFT). Based on these results, graphitic N might predominantly account for the ORR activity of N-doped carbon catalysts in alkaline electrolyte. Actually, several previous reports in the literature also reveal that graphitic N strongly influences on the ORR activity of N-doped carbons [46,47].

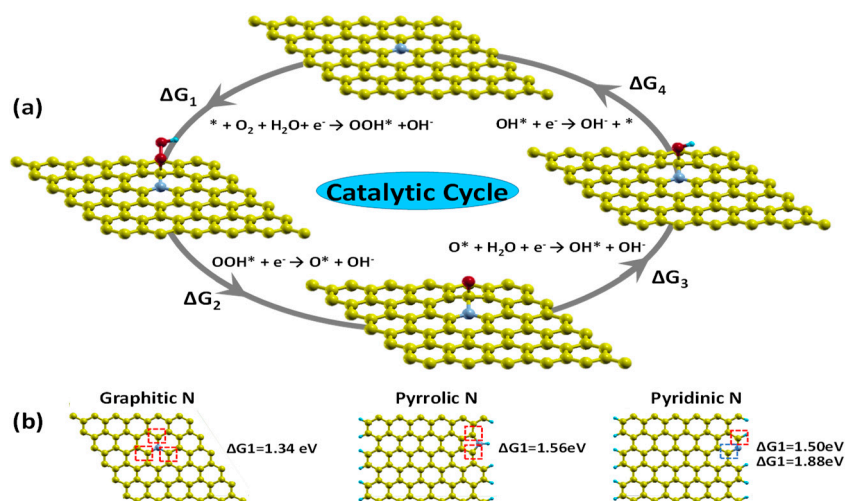


Figure 13. (a) Schematically showing the $4e^-$ reduction process of ORR proceeded on N-doped carbon. (b) The corresponding ΔG_1 values of the first-electron reduction process proceeded on carbon atoms surrounding different nitrogen doping configurations.

4. Conclusions

In summary, both experimental and theoretical approaches have been conducted to determine the ORR active sites of N-doped carbon catalysts. It is found that nitrogen doping induces charge redistribution on carbon skeletons. The introduction of an N atom that has a higher electronegativity than a C atom onto carbon skeletons creates charged sites which are favorable for oxygen chemisorption and enhances ORR activity. Besides intramolecular charge transfer induced by N-doping, intermolecular charge transfer induced by physical adsorption of polyelectrolytes also plays an important role in enhancing ORR activity among carbon-based nanomaterials. Additionally, topological defects and edge defects also demonstrate higher electrocatalytic activities than basal plane carbon for the ORR by modulating local electronic density and changing specific surface area.

Generally, introduction of N atoms into carbon materials not only can modulate the electronic distribution but also change the structure configuration, both of which may make a difference in the electrochemical activity and electrical conductivity. The content and location of specific N species directly influence the ORR activity performances. The thermal annealing temperature can tune the content of different nitrogen species within a carbon catalyst [48]. Transformation of pyrrolic N into a pyridinic N can be achieved at a relatively low annealing temperature whereas both pyrrolic and pyridinic N can be transformed into more stable quaternary N at high annealing temperatures [49]. The specific surface area also has an impact on ORR activity because the exposure of active sites are determined by porous structures and surface areas [50,51].

However, the vast majority of active site probing reports are based on bulk material analyses, for example XPS, which have limitations in obtaining signals at the atomic level, and hence direct microscopic evidence of active sites for ORR is unavailable. Generally, a mixture of many kinds of nitrogen species is obtained in one catalyst sample. In addition, it is usually compounded with structural parameters, including porosity, surface area, composition, morphology and degree of graphitization, which make it difficult to come to a consistent and also conclusive conclusion in active site probing results obtained by different groups. Therefore, the techniques for synthesizing carbon catalysts with mono-nitrogen doping configuration are still in early stages and more sophisticated

probing methods are desired concurrently to identify the active site and clarify the mechanism of ORR on N-doped carbons.

Author Contributions: N.Z., N.W. and L.L. wrote the paper; Z.W. helped revise the paper and edit the figures.

Acknowledgments: This work was supported by the National Natural Science Foundation of China (NSFC 51402111 and 21528301), Guangdong Innovative and Entrepreneurial Research Team Program (2014ZT05N200) and the Fundamental Research Funds for the Central Universities (SCUT Grant No. 2018ZD21).

Conflicts of Interest: The authors declare no conflict of interest.

References

1. Harper, C.; Snowden, M. *Environment and Society: Human Perspectives on Environmental Issues*; Taylor & Francis: Routledge, UK, 2017.
2. Sharaf, O.Z.; Orhan, M.F. An overview of fuel cell technology: Fundamentals and applications. *Renew. Sustain. Energy Rev.* **2014**, *32*, 810–853. [[CrossRef](#)]
3. Brito, P.S.D.; Sequeira, C.A.C. Cathodic oxygen reduction on noble metal and carbon electrodes. *J. Power Sources* **1994**, *52*, 1–16. [[CrossRef](#)]
4. Jiang, W.J.; Gu, L.; Li, L.; Zhang, Y.; Zhang, X.; Zhang, L.J.; Wang, J.Q.; Hu, J.S.; Wei, Z.; Wan, L.J. Understanding the high activity of Fe-N-C electrocatalysts in oxygen reduction: Fe/Fe₃C nanoparticles boost the activity of Fe-N(x). *J. Am. Chem. Soc.* **2016**, *138*, 3570–3578. [[CrossRef](#)] [[PubMed](#)]
5. Zhang, X.; Liu, R.; Zang, Y.; Liu, G.; Wang, G.; Zhang, Y.; Zhang, H.; Zhao, H. Co/CoO nanoparticles immobilized on Co-N-doped carbon as trifunctional electrocatalysts for oxygen reduction, oxygen evolution and hydrogen evolution reactions. *Chem. Commun.* **2016**, *52*, 5946–5949. [[CrossRef](#)] [[PubMed](#)]
6. Osgood, H.; Devaguptapu, S.V.; Xu, H.; Cho, J.; Wu, G. Transition metal (Fe, Co, Ni, and Mn) oxides for oxygen reduction and evolution bifunctional catalysts in alkaline media. *Nano Today* **2016**, *11*, 601–625. [[CrossRef](#)]
7. Zhang, Y.; Jiang, W.J.; Guo, L.; Zhang, X.; Hu, J.S.; Wei, Z.; Wan, L.J. Confining iron carbide nanocrystals inside CN_x@CNT toward an efficient electrocatalyst for oxygen reduction reaction. *ACS Appl. Mater. Interfaces* **2015**, *7*, 11508–11515. [[CrossRef](#)] [[PubMed](#)]
8. Yu, M.; Zhao, S.; Feng, H.; Hu, L.; Zhang, X.; Zeng, Y.; Tong, Y.; Lu, X. Engineering thin MoS₂ nanosheets on tin nanorods: Advanced electrochemical capacitor electrode and hydrogen evolution electrocatalyst. *ACS Energy Lett.* **2017**, *2*, 1862–1868. [[CrossRef](#)]
9. Chung, H.T.; Cullen, D.A.; Higgins, D.; Sneed, B.T.; Holby, E.F.; More, K.L.; Zelenay, P. Direct atomic-level insight into the active sites of a high-performance PGM-free ORR catalyst. *Science* **2017**, *357*, 479–484. [[CrossRef](#)] [[PubMed](#)]
10. Wang, H.F.; Tang, C.; Wang, B.; Li, B.Q.; Zhang, Q. Bifunctional transition metal hydroxysulfides: Room-temperature sulfurization and their applications in Zn-air batteries. *Adv. Mater.* **2017**, *29*, 1702327. [[CrossRef](#)] [[PubMed](#)]
11. Zhu, Y.; Zhou, W.; Zhong, Y.; Bu, Y.; Chen, X.; Zhong, Q.; Liu, M.; Shao, Z. A perovskite nanorod as bifunctional electrocatalyst for overall water splitting. *Adv. Energy Mater.* **2017**, *7*, 1602122. [[CrossRef](#)]
12. Jung, J.I.; Jeong, H.Y.; Lee, J.S.; Kim, M.G.; Cho, J. A bifunctional perovskite catalyst for oxygen reduction and evolution. *Angew. Chem.* **2014**, *53*, 4582–4586. [[CrossRef](#)] [[PubMed](#)]
13. Liu, X.; Dai, L. Carbon-based metal-free catalysts. *Nat. Rev. Mater.* **2016**, *1*, 16064. [[CrossRef](#)]
14. Wang, N.; Lu, B.Z.; Li, L.G.; Niu, W.H.; Tang, Z.H.; Kang, X.W.; Chen, S.W. Graphitic nitrogen is responsible for oxygen electroreduction on nitrogen-doped carbons in alkaline electrolytes: Insights from activity attenuation studies and theoretical calculations. *ACS Catal.* **2018**, *8*, 6827–6836. [[CrossRef](#)]
15. Gong, K.P.; Du, F.; Xia, Z.H.; Durstock, M.; Dai, L.M. Nitrogen-doped carbon nanotube arrays with high electrocatalytic activity for oxygen reduction. *Science* **2009**, *323*, 760–764. [[CrossRef](#)] [[PubMed](#)]
16. Zhang, L.; Xia, Z. Mechanisms of oxygen reduction reaction on nitrogen-doped graphene for fuel cells. *J. Phys. Chem. C* **2011**, *115*, 11170–11176. [[CrossRef](#)]
17. Kim, H.; Lee, K.; Woo, S.I.; Jung, Y. On the mechanism of enhanced oxygen reduction reaction in nitrogen-doped graphene nanoribbons. *Phys. Chem. Chem. Phys.* **2011**, *13*, 17505–17510. [[CrossRef](#)] [[PubMed](#)]

18. Zhou, T.; Zhou, Y.; Ma, R.; Zhou, Z.; Liu, G.; Liu, Q.; Zhu, Y.; Wang, J. Nitrogen-doped hollow mesoporous carbon spheres as a highly active and stable metal-free electrocatalyst for oxygen reduction. *Carbon* **2017**, *114*, 177–186. [[CrossRef](#)]
19. Singh, D.K.; Jenjeti, R.N.; Sampath, S.; Eswaramoorthy, M. Two in one: N-doped tubular carbon nanostructure as an efficient metal-free dual electrocatalyst for hydrogen evolution and oxygen reduction reactions. *J. Mater. Chem. A* **2017**, *5*, 6025–6031. [[CrossRef](#)]
20. Yadegari, A.; Samiee, L.; Tasharofi, S.; Tajik, S.; Rashidi, A.; Shoghi, F.; Rasoulianboroujeni, M.; Tahriri, M.; Rowley-Neale, S.J.; Banks, C.E. Nitrogen doped nanoporous graphene: An efficient metal-free electrocatalyst for the oxygen reduction reaction. *RSC Adv.* **2017**, *7*, 55555–55566. [[CrossRef](#)]
21. Kumar, M.P.; Raju, M.M.; Arunchander, A.; Selvaraj, S.; Kalita, G.; Narayanan, T.N.; Sahu, A.K.; Pattanayak, D.K. Nitrogen doped graphene as metal free electrocatalyst for efficient oxygen reduction reaction in alkaline media and its application in anion exchange membrane fuel cells. *J. Electrochem. Soc.* **2016**, *163*, F848–F855. [[CrossRef](#)]
22. Gong, K.P.; Chakrabarti, S.; Dai, L.M. Electrochemistry at carbon nanotube electrodes: Is the nanotube tip more active than the sidewall? *Angew. Chem. Int. Ed.* **2008**, *47*, 5446–5450. [[CrossRef](#)] [[PubMed](#)]
23. Shen, A.L.; Zou, Y.Q.; Wang, Q.; Dryfe, R.A.W.; Huang, X.B.; Dou, S.; Dai, L.M.; Wang, S.Y. Oxygen reduction reaction in a droplet on graphite: Direct evidence that the edge is more active than the basal plane. *Angew. Chem. Int. Ed.* **2014**, *53*, 10804–10808. [[CrossRef](#)] [[PubMed](#)]
24. Jia, Y.; Zhang, L.; Du, A.; Gao, G.; Chen, J.; Yan, X.; Brown, C.L.; Yao, X. Defect graphene as a trifunctional catalyst for electrochemical reactions. *Adv. Mater.* **2016**, *28*, 9532–9538. [[CrossRef](#)] [[PubMed](#)]
25. Zhao, X.J.; Zou, X.Q.; Yan, X.C.; Brown, C.L.; Chen, Z.G.; Zhu, G.S.; Yao, X.D. Defect-driven oxygen reduction reaction (orr) of carbon without any element doping. *Inorg. Chem. Front.* **2016**, *3*, 417–421. [[CrossRef](#)]
26. Yan, X.; Jia, Y.; Odedairo, T.; Zhao, X.; Jin, Z.; Zhu, Z.; Yao, X. Activated carbon becomes active for oxygen reduction and hydrogen evolution reactions. *Chem. Commun.* **2016**, *52*, 8156–8159. [[CrossRef](#)] [[PubMed](#)]
27. Jiang, Y.; Yang, L.; Sun, T.; Zhao, J.; Lyu, Z.; Zhuo, O.; Wang, X.; Wu, Q.; Ma, J.; Hu, Z. Significant contribution of intrinsic carbon defects to oxygen reduction activity. *ACS Catal.* **2015**, *5*, 6707–6712. [[CrossRef](#)]
28. Tao, L.; Wang, Q.; Dou, S.; Ma, Z.; Huo, J.; Wang, S.; Dai, L. Edge-rich and dopant-free graphene as a highly efficient metal-free electrocatalyst for the oxygen reduction reaction. *Chem. Commun.* **2016**, *52*, 2764–2767. [[CrossRef](#)] [[PubMed](#)]
29. Deng, D.H.; Pan, X.L.; Yu, L.A.; Cui, Y.; Jiang, Y.P.; Qi, J.; Li, W.X.; Fu, Q.A.; Ma, X.C.; Xue, Q.K.; et al. Toward n-doped graphene via solvothermal synthesis. *Chem. Mater.* **2011**, *23*, 1188–1193. [[CrossRef](#)]
30. Wang, S.Y.; Yu, D.S.; Dai, L.M.; Chang, D.W.; Baek, J.B. Polyelectrolyte-functionalized graphene as metal-free electrocatalysts for oxygen reduction. *ACS Nano* **2011**, *5*, 6202–6209. [[CrossRef](#)] [[PubMed](#)]
31. Wang, S.; Yu, D.; Dai, L. Polyelectrolyte functionalized carbon nanotubes as efficient metal-free electrocatalysts for oxygen reduction. *J. Am. Chem. Soc.* **2011**, *133*, 5182–5185. [[CrossRef](#)] [[PubMed](#)]
32. Gilli, G.; Bertolasi, V.; Bellucci, F.; Ferretti, V. Stereochemistry of the R1(x):C(sp2)-N(sp3)R2R3 fragment. Mapping of the cis-trans isomerization path by rotation around the carbon-nitrogen bond from crystallographic structural data. *J. Am. Chem. Soc.* **1986**, *108*, 2420–2424. [[CrossRef](#)] [[PubMed](#)]
33. Casanovas, J.; Ricart, J.M.; Rubio, J.; Illas, F.; Jiménez-Mateos, J.M. Origin of the large n 1s binding energy in X-ray photoelectron spectra of calcined carbonaceous materials. *J. Am. Chem. Soc.* **1996**, *118*, 8071–8076. [[CrossRef](#)]
34. Ding, W.; Wei, Z.; Chen, S.; Qi, X.; Yang, T.; Hu, J.; Wang, D.; Wan, L.J.; Alvi, S.F.; Li, L. Space-confinement-induced synthesis of pyridinic- and pyrrolic-nitrogen-doped graphene for the catalysis of oxygen reduction. *Angew. Chem.* **2013**, *52*, 11755–11759. [[CrossRef](#)] [[PubMed](#)]
35. Tang, C.; Wang, H.F.; Chen, X.; Li, B.Q.; Hou, T.Z.; Zhang, B.; Zhang, Q.; Titirici, M.M.; Wei, F. Topological defects in metal-free nanocarbon for oxygen electrocatalysis. *Adv. Mater.* **2016**, *28*, 6845–6851. [[CrossRef](#)] [[PubMed](#)]
36. Li, H.B.; Kang, W.J.; Wang, L.; Yue, Q.L.; Xu, S.L.; Wang, H.S.; Liu, J.F. Synthesis of three-dimensional flowerlike nitrogen-doped carbons by a copyrolysis route and the effect of nitrogen species on the electrocatalytic activity in oxygen reduction reaction. *Carbon* **2013**, *54*, 249–257. [[CrossRef](#)]
37. Yan, J.; Meng, H.; Xie, F.Y.; Yuan, X.L.; Yu, W.D.; Lin, W.R.; Ouyang, W.P.; Yuan, D.S. Metal free nitrogen doped hollow mesoporous graphene-analogous spheres as effective electrocatalyst for oxygen reduction reaction. *J. Power Sources* **2014**, *245*, 772–778. [[CrossRef](#)]

38. Park, M.; Lee, T.; Kim, B.S. Covalent functionalization based heteroatom doped graphene nanosheet as a metal-free electrocatalyst for oxygen reduction reaction. *Nanoscale* **2013**, *5*, 12255–12260. [[CrossRef](#)] [[PubMed](#)]
39. Liu, J.; Song, P.; Xu, W. Structure-activity relationship of doped-nitrogen (n)-based metal-free active sites on carbon for oxygen reduction reaction. *Carbon* **2017**, *115*, 763–772. [[CrossRef](#)]
40. Xing, T.; Zheng, Y.; Li, L.H.; Cowie, B.C.C.; Gunzelmann, D.; Qiao, S.Z.; Huang, S.M.; Chen, Y. Observation of active sites for oxygen reduction reaction on nitrogen-doped multilayer graphene. *ACS Nano* **2014**, *8*, 6856–6862. [[CrossRef](#)] [[PubMed](#)]
41. Friebel, J.; Kopsel, R.F.W. The fate of nitrogen during pyrolysis of german low rank coals—A parameter study. *Fuel* **1999**, *78*, 923–932. [[CrossRef](#)]
42. Guo, D.H.; Shibuya, R.; Akiba, C.; Saji, S.; Kondo, T.; Nakamura, J. Active sites of nitrogen-doped carbon materials for oxygen reduction reaction clarified using model catalysts. *Science* **2016**, *351*, 361–365. [[CrossRef](#)] [[PubMed](#)]
43. Li, B.; Sun, X.; Su, D. Calibration of the basic strength of the nitrogen groups on the nanostructured carbon materials. *Phys. Chem. Chem. Phys.* **2015**, *17*, 6691–6694. [[CrossRef](#)] [[PubMed](#)]
44. Metiu, H.; Chretien, S.; Hu, Z.P.; Li, B.; Sun, X.Y. Chemistry of lewis acid-base pairs on oxide surfaces. *J. Phys. Chem. C* **2012**, *116*, 10439–10450. [[CrossRef](#)]
45. Yang, H.B.; Miao, J.W.; Hung, S.F.; Chen, J.Z.; Tao, H.B.; Wang, X.Z.; Zhang, L.P.; Chen, R.; Gao, J.J.; Chen, H.M.; et al. Identification of catalytic sites for oxygen reduction and oxygen evolution in n-doped graphene materials: Development of highly efficient metal-free bifunctional electrocatalyst. *Sci. Adv.* **2016**, *2*, e1501122. [[CrossRef](#)] [[PubMed](#)]
46. Su, P.P.; Xiao, H.; Zhao, J.; Yao, Y.; Shao, Z.G.; Li, C.; Yang, Q.H. Nitrogen-doped carbon nanotubes derived from zn-fe-zif nanospheres and their application as efficient oxygen reduction electrocatalysts with in situ generated iron species. *Chem. Sci.* **2013**, *4*, 2941–2946. [[CrossRef](#)]
47. Nagaiah, T.C.; Kundu, S.; Bron, M.; Muhler, M.; Schuhmann, W. Nitrogen-doped carbon nanotubes as a cathode catalyst for the oxygen reduction reaction in alkaline medium. *Electrochem. Commun.* **2010**, *12*, 338–341. [[CrossRef](#)]
48. Panomsuwan, G.; Saito, N.; Ishizaki, T. Nitrogen-doped carbon nanoparticles derived from acrylonitrile plasma for electrochemical oxygen reduction. *Phys. Chem. Chem. Phys.* **2015**, *17*, 6227–6232. [[CrossRef](#)] [[PubMed](#)]
49. Stańczyk, K.; Dziembaj, R.; Piwowarska, Z.; Witkowski, S. Transformation of nitrogen structures in carbonization of model compounds determined by XPS. *Carbon* **1995**, *33*, 1383–1392. [[CrossRef](#)]
50. Liu, R.; Wu, D.; Feng, X.; Mullen, K. Nitrogen-doped ordered mesoporous graphitic arrays with high electrocatalytic activity for oxygen reduction. *Angew. Chem.* **2010**, *49*, 2565–2569. [[CrossRef](#)] [[PubMed](#)]
51. Liang, H.W.; Wei, W.; Wu, Z.S.; Feng, X.; Mullen, K. Mesoporous metal-nitrogen-doped carbon electrocatalysts for highly efficient oxygen reduction reaction. *J. Am. Chem. Soc.* **2013**, *135*, 16002–16005. [[CrossRef](#)] [[PubMed](#)]

